DOE/NASA/51044-29
NASA TM-83036

Tests of an Alternating Current Propulsion Subsystem for Electric Vehicles on a Road Load Simulator

Francis J. Stenger
National Aeronautics and Space Administration
Lewis Research Center

December 1982

Prepared for
U.S. DEPARTMENT OF ENERGY
Conservation and Renewable Energy
Office of Vehicle and Engine R&D

DOE/NASA/51044-29
NASA TM-83036

Tests of an Alternating Current Propulsion Subsystem for Electric Vehicles on a Road Load Simulator

Francis J. Stenger
National Aeronautics and Space Administration
Lewis Research Center
Cleveland, Ohio 44135

December 1982

Prepared for
U.S. DEPARTMENT OF ENERGY
Conservation and Renewable Energy
Office of Vehicle and Engine R&D
Washington, D.C. 20545
Under Interagency Agreement DE-AI01-77CS51044

TESTS OF AN ALTERNATING CURRENT PROPULSION SUBSYSTEM FOR ELECTRIC VEHICLES ON A ROAD LOAD SIMULATOR

Francis J. Stenger

National Aeronautics and Space Administration
Lewis Research Center
Cleveland, Ohio 44135

SUMMARY

An ac electric-vehicle-propulsion-subsystem breadboard was designed, built, and tested by the Eaton Corporation under a cost-shared contract to NASA Lewis Research Center as a part of the Department of Energy Electric and Hybrid Vehicle Program. The subsystem features an 18.65 kW ac induction motor, a pulse-width-modulated transistor inverter, a two-speed automatic transaxle, and a microprocessor-based controller.

The breadboard was subsequently delivered to NASA Lewis for additional steady-state and transient testing in the Road Load Simulator facility. These tests included acceleration tests and tests over the SAE J227a schedules B, C, and D driving cycles with full vehicle inertia simulation, which was not available for the Eaton testing. During the tests the Lewis Road Load Simulator was configured to simulate the characteristics of a modified Mercury Lynx passenger car of 1471-kg (3243 lb) mass. A reaction-type motor torque transducer was selected to permit a compact breadboard design. A transducer having the lowest available torque capacity was used, but this capacity was several times greater than the maximum motor torques measured. This excess transducer torque capacity resulted in a loss of accuracy in the low-torque-range measurements.

The greatest subsystem efficiency (inverter input to transaxle output) observed for the breadboard in the motoring mode was 81 percent in the low-gear speed range of the transaxle and 81.5 percent in the high-gear speed range. The greatest subsystem efficiency in the regenerative (braking) mode was 76 percent. The peak motoring efficiency of the motor-inverter combination was found to be 89 percent at high motor speeds and moderate torque levels.

During the driving schedule (transient) tests, the subsystem energy efficiency for the acceleration and cruise portion only of the SAE J227a schedules was determined to be

Schedule B, 49.2 percent
Schedule C, 58.3 percent
Schedule D, 68.4 percent

The control microprocessor was programmed with various developmental safety features to protect the breadboard from overstress during a maximum torque command at standstill. These safety features caused a time delay whenever attempts were made to start the motor from standstill and made it difficult to evaluate the maximum acceleration capability. However, simulated vehicle acceleration from 3.4 to 87 km/hr (2 to 54 mph) could be obtained in 33 sec. A Phase II contract with Eaton Corporation is presently underway to design, fabricate, and test an upgraded version of this propulsion system in a test vehicle.

E-1479

INTRODUCTION

The Electric and Hybrid Vehicle Program of the U.S. Department of Energy (DOE) provides for the development of advanced technology for electric and hybrid vehicle applications in order to maximize the potential of these transportation concepts. The DOE has delegated project management responsibility for the propulsion-subsystem-technology-development portion of this program to the NASA Lewis Research Center.

For some time, ac propulsion motor subsystems have formed an important segment of the DOE/Lewis propulsion technology program, and the potential simplicity and ruggedness of the ac motor continues to be attractive. During the late 1970's, interest in ac propulsion technology at the Eaton Corporation developed into a working relationship between Eaton and DOE/Lewis. In 1979 Eaton entered into a cost-shared contract with DOE/Lewis to develop the technology required for an ac propulsion subsystem for over-the-road electric vehicles. The initial phase of this project called for Eaton to design, build, and partially test a prototype of such a subsystem. The resulting engineering model breadboard features an 18.65-kW, oil-cooled, ac induction motor; a pulse-width-modulated (PWM) transistor inverter; a two-speed automatic transmission (transaxle); and a microprocessor-based controller. The design development of the breadboard and the results of the testing by the Eaton Corporation are reported in detail in references 1 and 2.

After testing at Eaton the breadboard was delivered to NASA-Lewis for additional steady-state and transient testing in the Road Load Simulator (RLS) facility. The transient tests included acceleration tests and tests over the SAE J227a schedules B, C, and D driving cycles using full vehicle inertia simulation which was not available at Eaton during their tests. For the Lewis tests the Road Load Simulator was configured to simulate a modified Mercury Lynx passenger car of 1471-kg (3243 lb) mass.

This report presents the results of the Lewis tests of the Eaton breadboard. The data presented fall into two main categories. First, steady-state data were obtained by operating the breadboard at a specific steady value of transaxle output torque and equivalent vehicle speed within the operating temperature range of the ac motor. The steady-state data presented concerns overall subsystem results, individual component results (inverter, motor, and transaxle), and selected variations in performance with dc source voltage and motor temperature.

Transient data form the second category, presented, for the most part, in the form of performance variables (subsystem efficiency, etc.) plotted as functions of time or equivalent vehicle speed. Data in this category were obtained from runs during which the breadboard was operated in a transient torque-speed mode to simulate execution of the SAE J227a schedules B, C, and D driving cycles and maximum accelerations from zero speed to 88.5 km/hr (55 mph).

SYMBOLS

C_dA aerodynamic drag coefficient - frontal area product for simulated vehicle, m^2

E energy, MJ

I_a accessory battery current, dc A

M mass, kg

P power, kW

R wattmeter reading

V voltage, dc V

v vehicle speed, km/hr

n efficiency, percent

Subscripts:

a accessory

b battery

bs battery, specific

ab accessory battery

i inverter

im combined inverter-motor value

in input

i1 phase one of inverter output

i2 phase two of inverter output

m motor

t total (for subsystem)

ta transaxle

s subsystem (with accessory)

sb subsystem (with traction battery only)

EXPERIMENTAL PROPULSION SUBSYSTEM

Figure 1 is a simplified block diagram of the experimental ac breadboard to be tested. The upper solid lines show the flow of power through the subsystem from the main 144-V dc traction power supply to the vehicle wheels. The lower power flow path (lower solid line) represents the control power into the subsystem controller, the hydraulic oil pump, and control valves (not shown). The dashed paths represent the major control-command functions in the subsystem.

The function blocks shown in figure 1, except for the controller, represent the major components mounted on the breadboard structure as supplied to Lewis for testing. Figure 2 is a photograph of these components installed in the RLS facility. The breadboard controller, which does not appear in this photograph, was installed in an adjacent instrumentation and control room.

Figure 2 also shows some other important components of the breadboard which do not appear in the diagram of figure 1. The largest of these is the dc switchbox, which houses the main dc bus-circuit contactor. The dc input connector on the upper right exterior of the switchbox allows either the 144-V dc traction battery or laboratory power supply to be connected to the breadboard. The connector contains a safety interlock to prevent main contactor closure without a secure "make" of the connector. The oil cooler, oil pump,

and oil control subassembly components are partiall, ible at the lower left of the switchbox in figure 2. This subassembly provides cooled oil under pressure for lubrication and cooling in the induction motor and the transaxle. The oil is also used, via electric solenoid valves, to actuate two clutches within the transaxle to select either of two speed ratios.

A detailed description of the ac breadboard and its components may be found in references 1 and 2. Some of the major component specifications from reference 2 are summarized in table I.

TEST APPARATUS

Road Load Simulator

The basic test facility used for these tests at Lewis is the Road Load Simulator. The RLS is a special purpose dynamometer system capable of applying road-load torque to a propulsion system, thereby duplicating the torque that the system would normally experience in vehicle operation. This general facility has been described in detail in reference 3 and its application to the testing of the Near-Term Electric Vehicle (ETV-1) Breadboard Propulsion System is discussed in references 4 and 5. The major components of the RLS are shown in figure 3, which has been reproduced from reference 4. The drive motor and the absorber clutch provided the steady-state components of the road load torque. The right-angle gear unit just to the right of the absorber clutch (fig. 3) was removed and replaced by a simple shaft for this testing to reduce mechanical losses in the system. The inertia wheels were retained to provide the inertial component of the road load. The low-speed gear box was used as shown to provide the proper wheel-axle input speed for the experimental propulsion subsystem. The torque meter shown to the right of the low speed gear box in figure 3 corresponds to the wheel-axle torque transducer identified in figure 2.

For these tests the battery simulator represented either of two distinct types of dc power supplies. One power supply was an adjustable-voltage motor-generator set with a capacitive filter network. This power supply was used to obtain the steady-state, nonregenerative data. The second power supply was a group of 24 EV-106 lead-acid traction-batteries series connected to produce a nominal 144 V dc. This battery set was used for all transient testing over SAE J227a driving schedules, for maximum acceleration tests, and for most of the regenerative braking testing.

The RLS has only a single shaft to couple with an experimental propulsion subsystem. Since the ac propulsion subsystem contains an automotive-type differential gear and two axle shafts, this gearing locked to permit all the traction torque to be transmitted to the RLS through a single-axle shaft.

Instrumentation

The basic instrumentation and computer-controlled automatic data acquisition system used for these tests is discussed in reference 3. Wide-band coaxial current shunts and electronic wattmeters were used in the electrical power circuits. The three-phase electric power transmitted between the inverter and the motor was measured using two wattmeters.

The transaxle output (wheel) torque was measured with a conventional in-line torque sensor visible in figure 2. To measure motor-shaft torque, a

flanged reaction torque sensor was mounted between the motor case and the transaxle housing (see fig. 2). This type of sensor was used to minimize additional mechanical loss and undesirable dynamic effects in the 9000-rpm (maximum) motor shaft. However, this type of torque sensor was not readily available in a full-scale torque capacity less than 225 N-m, which is about four times the maximum motor torque. Dead-weight static torque calibration of the complete torque measurement system showed the motor torque error band to be about ±0.226 N-m. An additional error in the motor torque measurement was a temperature-induced zero drift of the torque sensor caused by the heating of the motor-side torque-sensor flange as the motor temperature increased during the test runs. The data were corrected for this error but an additional error band of about ±0.22 N-m in the motor torque data resulted. Thus, the total error band for the motor-torque data is estimated to be ±0.446 N-m, or about ±0.82 percent of the 54.2 N-m maximum expected torque.

The motor-case temperature (used as a test reference) was measured by an outer-surface thermocouple installed in the top center of the motor case with the motor oriented as shown in figure 2.

TEST PROCEDURE

Steady-State Tests

The basic approach for the steady-state tests was to select an equivalent vehicle speed and a wheel axle torque and then run the breadboard at this condition (constant wheel power) for an extended time, usually 1 to 2 hr. As the subsystem temperatures increased, a complete scan of all data elements was recorded at selected intervals of time. A variation of this procedure, used for many of the test points, was to move back and forth between two or three torque values and record data scans at each value to produce data curves at multiple torque values during a single system temperature excursion. The motor-case temperature was used as a test reference because the subsystem efficiency was expected to be most sensitive to this temperature. During the steady-state testing the motor case temperature varied in the range 24° to 150° C.

For the steady-state tests, a battery simulator voltage of 144 V dc was used as a standard. In addition to 144 V dc, selected speed-torque points were also run at 124 and 104 V dc to study the effect of battery voltage variation on subsystem performance.

Figure 4 shows a map of the nominal speed-torque test points investigated. The test points at torque values greater than zero represent motoring points with power flow from the breadboard to the RLS (the simulated vehicle). Limited motoring runs made with the EV-106 traction batteries verified the adequacy of the battery simulation by the filtered motor-generator set.

The test points on figure 4 at torque values less than zero represent regenerative braking points with power flow from the RLS through the breadboard back into the traction battery.

All test points on or to the left of the vertical dashed line in figure 4 were run with the transaxle in low gear (overall ratio from motor shaft to wheel axle = 19.7:1). All test points to the right of the line, with speeds greater than 45 km/hr, were run in high gear (overall ratio = 8.22:1). The set of test points connected by the solid curve labeled "road-load torque line" defines the wheel-axle speed-torque characteristics of the simulated

vehicle at steady speed with no wind on a level road. A speed torque-power cross reference is presented in table II to interrelate the simulated vehicle speed with the motor-shaft speed and the wheel-axle speed, torque, and road-load power.

Transient Tests

Tests were run to characterize the breadboard's performance while executing SAE J227a B, C, and D driving schedules and while accelerating as near to maximum conditions as could be managed using a very simple control interface between the RLS driving-schedule programmer and the breadboard system. The command signal to the breadboard controller was an acceleration (positive) torque signal or a deceleration or braking (negative) torque signal. The source of the command signal was the RLS driving-schedule control system, which compares the actual vehicle speed with the desired preprogrammed value and generates the appropriate torque command. A delay in the response of the breadboard to a torque command at near-zero speed occurred because a maximum torque command signal at zero motor speed would produce only a small fraction of rated motor torque. To address this problem, the preprogrammed driving schedules were tailored in the initial near-zero speed regions to provide actual speed-time profiles suitably close to the standard SAE profiles.

Power Measurements and Calculations

The most important test data derived from the specific measurements were the power levels at various points along the subsystem energy flow paths. These important power points are illustrated in block-diagram form in figure 5. The power symbols used are defined in the symbol list.

The power flow to the system from the accessory battery requires some explanation. During the testing, the accessory-battery output power P_{ab} was computed from the total current and associated voltage input to the test system. During the tests the accessory battery was continuously charged by a conventional 12-V automotive battery charger. The loss in this 12-V charger was probably less than 0.05 kW and was not charged to the subsystem. Two cooling fans in the three-phase inverter operate from 120-V ac, 60-Hz line power. The combined rated power of both fans is 0.16 kW, as noted in figure 5. The accessory power for the subsystem P_a is defined as the sum of P_{ab} and a constant 0.16 kW for the cooling fans. Specifically, P_a is the power consumed by the subsystem controller, the hydraulic pump, the solenoid hydraulic control valves, and the inverter cooling fans.

The battery (or battery simulator) output power P_b was directly recorded from a wideband electronic wattmeter. In a similar way, the motor-shaft power P_m and the transaxle-output-shaft power P_{ta} were recorded as the output from an electronic analog multiplier which formed the product of the associated shaft speed, torque, and units constant.

The inverter output power P_i was computed as the sum of the wattmeter readings in Phase 1 (R_{i1}) and Phase 2 (R_{i2}) of the three-phase inverter output leads; or

$$P_i = R_{i1} + R_{i2}$$

where R is used for a wattmeter reading and does not indicate an actual phase power. The output power P_{ab} of the 12-V accessory battery was

computed as the product of the accessory-battery output current I_a and the voltage V_a, or

$$P_{ab} = I_a V_a$$

To compute P_a, the assumed constant-inverter-cooling fan power, 0.16 kW, was added to P_{ab}, or

$$P_a = P_{ab} + 0.16$$

The total power consumption P_t for the breadboard was defined as the sum of the battery power and the accessory power, or

$$P_t = P_b + P_a$$

Efficiency Calculations

The breadboard component and subsystem efficiencies were calculated using the general relationship:

$$\eta = \frac{P_{out}}{P_{in}}$$

where

η efficiency
P_{out} power output
P_{in} power input

Using this relationship, the following specific efficiencies were computed:

$$\text{Inverter efficiency } (\eta_i) = 100 \times \frac{P_i}{P_b} \text{ percent}$$

$$\text{Motor efficiency } (\eta_m) = 100 \times \frac{P_m}{P_i} \text{ percent}$$

$$\text{Transaxle efficiency } (\eta_{ta}) = 100 \times \frac{P_{ta}}{P_m} \text{ percent}$$

and

$$\text{Subsystem efficiency } (\eta_s) = 100 \times \frac{P_{ta}}{P_t} \text{ percent.}$$

Because it is often useful to consider the combined efficiency of the inverter and motor η_{im}, this efficiency was defined and computed as

$$\eta_{im} = 100 \times \frac{P_m}{P_b} \text{ percent}$$

Efficiencies during regenerative braking are computed using these equations, but with the power ratios shown replaced by their reciprocals. In particular, the total system power P_t during regenerative braking is the sum of a negative battery power (the battery is being charged) P_b and an always positive accessory power P_a. Thus, since P_{ta} is negative during regenerative braking, the system efficiency will be negative if

$$|P_b| < P_a$$

which indicates that net battery energy is being supplied to the system even though regenerative braking is in progress.

Energy Integrations

Energy consumption for selected driving schedules and acceleration maneuvers was computed by integrating the particular power over time.

Vehicle Simulation

The road-load simulation functions of the RLS were set to simulate a modified 1981 Mercury Lynx vehicle, which is representative of the class of vehicles which could be fitted with an electric propulsion subsystem of the type tested. The necessary numerical parameters used to define the vehicle are listed in table III. Note that a vehicle mass of 1471 kg was used to compute the tire-friction component of road load. However, during the time period between the steady-state and transient tests, a bearing failure occurred in the RLS inertia wheel system. Repairing the failure when it occurred was not cost effective. Thus, for the transient tests, the vehicle inertial mass was set at 1568 kg, which was the setting nearest to the 1471-kg value that could be achieved with the failed bearing. The bearing problem in no way affected the RLS operation, other than to restrict the inertia set point. The 1471-kg mass corresponds to a vehicle carrying two passengers, while 1568 kg would represent a payload of between three and four passengers. This test-mass difference was judged acceptable for this test series.

RESULTS AND DISCUSSION

Steady-State Tests

The ac breadboard tests are reported as system characterization tests with vehicle speed and transaxle-output (wheel axle) torque as the primary independent parameters. The effect of battery voltage and overall component temperature is also discussed. The data are presented under the following five subheadings: General steady-state results, Component performance, Battery voltage effects, Temperature effects, and Regenerative braking characteristics.

General steady-state results. - This section deals with results from test points at positive transaxle-torque levels shown in figure 4.

In figure 6 the subsystem efficiency is presented as a function of vehicle speed for a number of constant transaxle-torque values. (The vertical line at 45 km/hr in figure 6 marks the approximate boundary between low-gear and

high-gear operating regions.) The broken line shows the subsystem efficiency at the road-load transaxle torques characteristic of steady-speed operation of the vehicle on a level road with no wind. The dotted curve, reproduced from reference 5, shows the efficiency of the ETV-1 breadboard for its particular road-load conditions.

Figure 6 shows the increase in subsystem efficiency, at a constant transaxle torque, as the vehicle speed (thus, the motor speed and inverter frequency) increases in each of the two gear ratios (low and high). As the speed increases, the subsystem losses increase more slowly than the output power and efficiency rises. In low gear, for the torque values plotted in figure 6, the subsystem efficiency continues to increase as shift point (45 km/hr) is approached. However, in high gear the efficiency reaches a maximum at or slightly above a speed of 90 km/hr.

The ac breadboard has a 3- to 7-percent efficiency advantage over the dc ETV-1 breadboard in the low-speed range (<45 km/hr) and again near 90 km/hr. On the other hand, the ETV-1 shows a significant advantage in the 50 to 80 km/hr range.

Figure 7 presents the subsystem efficiency as a function of transaxle torque for constant vehicle speeds (fig. 7(a) for low gear speeds, fig. 7(b) for high gear speeds). In this form of presentation, the discontinuity due to gear change is not as apparent as it is for the curves shown in figure 6. The data of figure 6 was taken at a motor temperature of 43.3° C (110° F) to compare to the data from ETV-1 tests (ref. 5). Figure 7 shows data obtained at a motor temperature of 65.6° C (150° F), which is more representative of a normal operating temperature for the Eaton motor. At a steady speed of 72.4 km/hr (45 mph) (fig. 7(b)), the subsystem efficiency has a maximum of about 80 percent at a transaxle torque near 300 N-m (2655 lb-in). However, at the steady-speed road load torque of 88.1 N-m (780 lb-in), the subsystem efficiency is only 68 percent. This decrease in efficiency at lower output torques is typical of vehicle propulsion systems in general.

Estimating the range of an electric vehicle at a particular steady speed is common. If S is the range of a vehicle in kilometers at the steady speed v in kilometers per hour, then

$$S = \frac{1}{3.6} v \frac{E_{bs} M_b}{P_b}$$

where

E_{bs} battery specific energy, MJ/kg

M_b total battery mass, kg

P_b required battery power, kW

In figure 8, battery-simulator power and current from the steady-state tests are plotted as functions of steady vehicle speed on a level road with no wind for the simulated vehicle parameters listed in table III. With the aid of this figure, the range of the simulated vehicle can be estimated. For example, at a steady speed of 72.4 km/hr, the required battery power of 9.5 kW can be read from figure 8. For a battery mass, M_b, of 392 kg (table III) having a specific energy E_{bs} of 0.126 MJ/kg, the range is calculated from the above equation to be 105 km.

In figure 9, battery power is plotted as a function of vehicle speed on lines of constant transaxle torque neglecting component temperature effects.

Component performance. - Figures 10 to 13 are plots of selected performance data for the breadboard components; these figures are also plots of efficiency as a function of transaxle torque for constant vehicle speeds from 8.05 to 96.5 km/hr (5 to 60 mph). To minimize the impact of the zero drift as discussed under Test Apparatus, figures 11 to 13 were prepared from data at a motor temperature of 37.8° C (100° F), which provided both an adequate number of test points and a low zero-drift impact. Since the inverter power readings did not involve the motor torque transducer, figure 10 was plotted using 65.6° C (150° F) motor-temperature test points to be consistent with the subsystem plots in figures 7 and 8.

In figure 10(a) (the low-gear speed range), the vehicle speeds shown cover a range of 5 to 1, from 40.2 to 8.05 km/hr (25 to 5 mph). For the same vehicle-speed range, the motor-shaft speed (see table III) varies from 825.6 to 165.0 rad/sec (7884 to 1576 rpm). A significant drop in inverter efficiency occurs as either vehicle speed or transaxle torque decreases. The maximum inverter efficiency observed was 94.5 percent at 40.2 km/hr and a transaxle torque of 452 N-m (4000 lb-in). The minimum inverter efficiency observed was about 47 percent at 8.05 km/hr at the road load torque of 37 N-m. In figure 10(b) a similar set of curves is presented for operation in the high-gear speed range. The vehicle-speed range for this data is 1.71 to 1, with a motor-shaft speed range from 826.7 to 482.2 rad/sec (7894 to 4605 rpm).

The motor-efficiency data presented in figure 11(a) illustrate the accuracy problem with the motor torque transducer as discussed in the Test Apparatus section. The error band is shown in figure 11(a) for the 40.2-km/hr curve. Caution must be exercised in interpreting data below transaxle torque values of 340 N-m (3000 lb-in).

The efficiency data for the combined motor-inverter are presented in figure 12 and for the transaxle in figure 13. The same low-torque accuracy problem discussed for figure 11 applies to these figures.

Battery voltage effects. - The effects of operating the breadboard over the voltage range from 104 to 144 V are shown in figures 14 to 17. For these figures data acquired at a simulated vehicle speed of 72.4 km/hr (45 mph) were selected as representative of the major effects observed.

In figure 14 the battery-simulator current is plotted as a function of battery-simulator voltage for transaxle-torque values of 113 and 226 N-m (1000 and 2000 lb-in). Since the constant torque lines at the single vehicle speed shown (72.4 km/hr) are also constant transaxle-power lines, the battery-simulator current would be expected to increase along these lines as the voltage decreases. This trend is evident in figure 14. Figure 15 shows that the constant torque lines are approximately constant battery power lines. For the 113-N-m torque curve, the battery-simulator power drops from 11.5 kW at 144 V to 10.5 kW at 104 V. The 226-N-m torque curve exhibits a slight minimum between 125 and 130 V.

The general trends observed for the inverter efficiency in figure 16 are consistent with the plot of battery-simulator power of figure 15. Where the inverter efficiency is high (fig. 16), the battery power is low (fig. 15). The impact of the inverter efficiency variations with battery voltage is clearly visible in the subsystem efficiency plotted as a function of battery-simulator voltage in figure 17.

Temperature effects. - The motor-case temperature was used as a reference temperature during the tests as discussed in the Test Procedure section. Since this temperature measurement point is somewhat isolated from the motor

windings and rotor, the correlation of efficiency against motor case temperature was expected to show only general trends.

In figure 18, the subsystem efficiency is plotted as a function of motor-case temperature on lines of constant vehicle speed for a transaxle torque of 113 N-m (1000 lb-in). The variation of subsystem efficiency with temperature is low, except for the 8.05-km/hr curve in figure 18(a). In this case, most of the efficiency variation in this curve was caused by variation in the accessory power load. The battery-simulator output power varied only from 2.20 to 2.25 kW over the same temperature range (indicating an almost-constant traction-power requirement).

Data recorded at the higher transaxle torque value of 226 N-m are shown in figure 19 for the high-gear speed range only. Here, the subsystem efficiency decreases somewhat with increasing motor-case temperature. The system efficiency drops from two to three efficiency points over the temperature range shown in figure 19. Motor data (not shown) support the conclusion that this slight subsystem efficiency drop is attributable to an associated drop in motor efficiency as the motor temperature rises. The inverter efficiency was determined to be only a negligible function of motor-case temperature, and no data are shown.

Regenerative braking characteristics. - The regenerative braking tests were performed using EV-106 batteries (see Test Apparatus) at a 60-percent state-of-charge (SOC). These batteries had a measured capacity of 117 A-hr, somewhat below the nominal value of 132.5 A-hr for the EV-106. More importantly, the battery characteristics were different than those of the battery for which the subsystem was designed. Therefore, figures 20 to 22 are more useful for indicating trends rather than exact performance. This is especially true for figure 22, which involves battery current, a much stronger function of the battery characteristics than are efficiency and power.

In figure 20, the regenerative-braking subsystem efficiency is shown as a function of vehicle speed (in low-gear speed range only) on lines of constant transaxle torque. Note that a negative efficiency is shown for the -113 N-m torque curve. A negative efficiency in the regeneration mode means that the net output power of the traction batteries plus the accessory battery was positive, even though the transaxle torque was negative, i.e., the flow of power is from battery to motor. The peak regenerative subsystem efficiency recorded, 71 percent, occurred at a transaxle torque of -452 N-m and a vehicle speed of 40.2 km/hr. In general, for a given vehicle speed and transaxle-torque magnitude, the breadboard is less efficient in the regenerative braking mode than in the driving mode. This lower regenerative efficiency is consistent with the results presented in reference 2 for the combined efficiency of the motor and inverter.

In figures 21 and 22, the regenerative battery power and the regenerative battery current, respectively, are plotted as functions of vehicle speed on lines of constant transaxle braking torque. The battery current shown in figure 22 is the average value of a current waveform which contained a significant ripple component.

Transient Tests

The subsystem efficiency plots (figs. 28 and 33) show a number of points with indicated efficiency of 100 percent. These efficiency values are invalid and result from a limitation of the computer program in calculating efficiency from data during very rapid accelerations. When the traction motor speed rapidly decelerates, its output shaft power can, due to inertia, exceed its

electrical input power for a brief period. When this occurred (as during a transaxle gear shift, etc.), the computer program computed efficiencies in excess of 100 percent. All points shown at 100 percent should be ignored as true efficiency values.

SAE J227a driving schedule tests. - The data presented in this section characterize the breadboard's performance over the acceleration and cruise portion of representative single driving cycles.

Figures 23 to 28 present the significant parameters of the system during a representative Schedule D cycle. The vehicle speed profile is shown in figure 23. The onset of the transaxle shaft motion occurred at 5 sec after zero reference time. The shift points of the transaxle from low to high gear and high to low gear are indicated in the figure.

The transaxle torque is shown in figure 24. The data points at 3 and 4 sec are a result of the somewhat erratic starting torques, prior to onset of motion, characteristic of the breadboard's operation during the RLS tests. The downward torque spike at 20 sec coincides with the upshift operation of the transaxle. The large negative torque spike at 99 sec occurred immediately after transaxle downshift.

An attempt was made to follow a constant power-acceleration profile from zero speed to 72.4 km/hr (45 mph). The plot of the battery power shown in figure 25 indicated that a power near 25 kW was sustained for about 50 percent of the acceleration time The battery-current profile is shown in figure 26 and corresponds to the battery-power profile.

The transaxle power in figure 27 reflects the same general trends as the battery-power profile. The ratio of the transaxle power to the battery-power subsystem efficiency is plotted in figure 28. The efficiency values shown during the first 5-sec time interval should be disregarded, since they occur at very low power levels during the start-up lag discussed above and are highly in error. A similar problem exists just after the cruise portion of the cycle at about 84 sec. Rapid inertial transients and transaxle clutch actuations result in large errors in the efficiency calculation. Only the portion of the curve between 5 and 84 sec should be considered. The maximum system efficiency during the D cycle, about 76 percent, occurs during vehicle acceleration at an indicated time of 15 sec in low gear and again during the time interval from 28 to 34 sec in high gear. The average system efficiency during the 72.4-km/hr cruise portion of the cycle was about 67 percent.

Figure 29 is a plot of battery voltage as a function of battery current during the execution of the D cycle.

In figures 30 and 31, vehicle speed is plotted as a function of time for representative Schedule C and B cycles, respectively. For the C cycle (fig. 30), the transaxle upshifted to high gear at about 28 sec, just before the cruise speed of 48.3 km/hr (30 mph) was achieved. However, for the B cycle (fig. 31), the transaxle never shifted and the complete cycle was run in low gear.

Energy values were computed by integrating power (see fig. 4) over time during the motoring (acceleration and cruise) portion of the Schedule D, C, and B cycles. The results for the energy out of the battery and the energy at the transaxle shaft, along with the associated subsystem motoring efficiencies, are presented in table IV. The subsystem motoring efficiency with accessory energy η_S included for the D cycle is listed in table IV as 68.4 percent. This may be compared with the maximum transient subsystem efficiency during the D cycle of 76 percent observed in figure 28. The corresponding efficiencies for the B and C cycles are 49.2 and 58.3 percent, respectively.

Performance tests. The acceleration tests were performed to indicate general subsystem performance and do not include possible variations due to battery state-of-charge. Therefore, only data obtained with a battery SOC near 100 percent are reported in the following figures.

Figure 32 is a plot of vehicle speed as a function of time during a maximum acceleration to 88.5 km/hr (55 mph) on a zero percent simulated road grade at a battery SOC of 95 percent. The acceleration was maximum in the sense that the detailed shape of the command signal to the controller was adjusted so that the breadboard would execute the acceleration without an automatic shutdown from any of the microprocessor-controlled limit conditions (ref. 2). The best time from zero to 88.5 km/hr was 40 sec. However, when the various control-related compromises (command signal versus shutdown limits, etc.) are considered, the breadboard should be capable of accelerating a vehicle to 88.5 km/hr in about 35 sec. The drop in vehicle speed after 54 sec was preprogrammed into the speed-command profile.

The subsystem efficiency is plotted as a function of time in figure 33 for the above acceleration. During this acceleration the peak efficiency (ignoring the 100 percent data points) achieved was slightly over 77 percent at a time of 44 sec. The battery power is shown in figure 34 with a peak value of 33 kW at a time of 38 sec.

Figure 35 is a plot of vehicle speed versus time during maximum acceleration on a simulated road grade of 4 percent. The breadboard reached a simulated vehicle speed of 80.5 km/hr (50 mph) in 34 sec on the grade, but the maximum speed was 87.7 km/hr (54.5 mph), slightly less than the 88.5 km/hr objective.

SUMMARY OF RESULTS

The Eaton Corporation Phase 1 ac propulsion subsystem breadboard was tested at Lewis on the Road Load Simulator to characterize its performance both at steady state and under transient conditions (SAE J227a schedules and maximum accelerations). The following general results were obtained:

Steady-State Tests

(The speed and torque pairs used below refer to the simulated vehicle speed and the transaxle output torque.)

1. The peak subsystem efficiency observed for the breadboard was 81 percent in the low-gear speed range at a speed of 40.2 km/hr (25 mph) and a torque of 340 N-m (3000 lb-in); and 81.5 percent in the high-gear speed range at 88.5 km/hr (55 mph) and 170 N-m (1500 lb-in).
2. The traction battery power required by the simulated vehicle (1471-kg test mass) with this propulsion subsystem at a steady speed of 72.4 km/hr (45 mph) on a level road was 9.5 kW.
3. The peak inverter efficiency was 94.5 percent at a speed of 96.5 km/hr (60 mph) and a torque of 170 N-m (1500 lb-in). The lowest inverter efficiency observed was 48 percent at 8.05 km/hr (5 mph) and 37.2 N-m (329 lb-in).
4. The peak combined efficiency of the motor and inverter was 89 percent at 40.2 km/hr (25 mph) and 271 N-m (2400 lb-in).
5. The peak low-gear-range transaxle efficiency was 94 percent at 40 km/hr (25 mph) and 226 N-m (2000 lb-in), while the high-gear-range peak efficiency was 97 percent at 56.3 km/hr (35 mph) and 283 N-m (2500 lb-in).

6. In general, the system efficiency of the breadboard during regenerative braking was less than during motoring. In particular, the maximum regenerative system efficiency observed during the Lewis tests was 76 percent at 40.2 km/hr and -452 N-m (-4000 lb-in) in the low-gear transaxle ratio.

Driving Schedule and Performance Tests

1. Subsystem energy efficiency for the acceleration and cruise portion only of the SAE J227a Schedules B, C, and D was as follows:

Schedule B, 49.2 percent
Schedule C, 58.3 percent
Schedule D, 68.4 percent

These efficiencies were computed using the ratio of transaxle output energy divided by the battery output energy (including accessory energy).

2. Under maximum acceleration with a fully charged (95-percent SOC) battery, the breadboard required 40 sec to reach a simulated 88.5 km/hr (55 mph) from zero speed. Reflecting the slow-start characteristic of the breadboard, the 3.4 to 87 km/hr (2 to 54 mph) time for the same acceleration required 33 sec.

REFERENCES

1. Geppert, S.: AC Propulsion System for An Electric Vehicle. Presented at the Convergence '80 Conference, (Detroit, MI), Sept. 15-18, 1980.
2. Geppert, S.: AC Propulsion System for An Electric Vehicle. (ERC TR-8101, Eaton Corporation; NASA Contract DEN3-125.) DOE/NASA/0125-1, NASA CR-165480, Aug., 1981.
3. Sargent, N. B.: A Laboratory Facility for Electric Vehicle Propulsion System Testing. DOE/NASA/1011-32, NASA TM-81574, Sept., 1980.
4. Sargent, N. B.; and Dustin, M. O.: Characterization of the Near-Term Electric Vehicle (ETV-1) Breadboard Propulsion System Over the SAE J227a Driving Schedule D. DOE/NASA/51044-15, NASA TM-81664, Feb., 1981.
5. Sargent, N. B.; and Dustin, M. O.: Results of the ETV-1 Breadboard Tests Under Steady-State and Transient Conditions. DOE/NASA/51044-21, NASA TM-82667, Oct. 1981.

TABLE I. - EXPERIMENTAL ac PROPULSION SUBSYSTEM
COMPONENT SPECIFICATION SUMMARY

Inverter:	
Type[a]	PWM, three phase
Rating[b], kW	30
Input bus voltage, V dc	94 to 160
Maximum equivalent transistor switching rate, kHz	2
Motor:	
Type[c]	ac induction, traction
Rating, kW -	
For 1 hr at or above base speed	18.6
For 2 min at base speed	33.6
Base speed, rad/sec (rpm)	591 (5640)
Maximum speed, rad/sec (rpm)	942 (9000)
Weight (dry), kg	66.8
Transaxle:	
Type[d]	two speed
Rating, kW -	
Continuous	18.6
Intermittent	33.6
Overall ratios -	
Low gear	19.7:1
High gear	8.22:1
Weight with hydraulic controls (wet), kg	48
Controller:	
Type[e] (microprocessor based)	slip control scheme

[a]With 300-V, 400-A monolithic Darlington transistor power switches.
[b]Current limit to lower power at slow speed.
[c]Three-phase, two-pole, oil cooled
[d]Automatic shift by electric solenoid valve hydraulic clutches.
[e]PWM voltage control with constant volts per hertz up to base speed;
six-step, constant voltage variable frequency control above base speed.

TABLE II. - SPEED TORQUE-POWER CROSS REFERENCE

Gear[a]	Vehicle speed		Motor-shaft speed		Wheel-axle parameters[b]			
					Speed		Torque	Power
	km/hr	mph	rad/s	rpm	rad/s	rpm	N-m	kW
Low	8.1	5	165.0	1576	8.38	80.0	37.2	0.31
	16.1	10	330.3	3154	16.76	160.1	39.1	.66
	24.1	15	495.3	4730	25.13	240.1	42.3	1.06
	32.2	20	660.4	6306	33.52	320.1	46.8	1.57
	40.2	25	825.6	7884	41.91	400.2	52.4	2.20
High	56.3	35	482.2	4605	58.66	560.2	67.8	3.98
	72.4	45	620.0	5921	75.43	720.3	88.1	6.65
	88.5	55	757.8	7236	92.18	880.3	113.6	10.47
	96.5	60	826.7	7894	100.57	960.4	128.3	12.90

[a]Overall gear ratio, motor-to-wheels: low, 19.7:1; hig, 8.22:1.
[b]At steady speed on level road with no wind.

TABLE III. - SIMULATED VEHICLE PARAMETERS

Vehicle test mass[a,b], kg	1471
Tire friction, N/N	0.0095
Aerodynamic losses (C_dA), m^2	0.838
Rolling radius, m	0.2667

[a]Assumed battery mass = 392 kg.

[b]1568-kg inertia mass for all driving schedule and acceleration tests; see text.

TABLE IV. - SUMMARY OF DRIVING-SCHEDULE-TEST ENERGY DATA

For acceleration and cruise portion of cycle only:	Schedule B	Schedule C	Schedule D
Battery terminal energy plus accessory energy, E_t, Out, MJ (Wh)	0.242 (67)	0.415 (115)	1.071 (297)
Battery terminal energy only, E_b, Out, MJ (Wh)	0.228 (63)	0.403 (112)	1.050 (292)
Energy at transaxle output shaft, E_{ta}, Out, MJ (Wh)	0.119 (33)	0.242 (67)	0.733 (204)
Subsystem motoring efficiency including accessory energy, $n_s = 100 \times E_{ta}/E_t$, percent	49.2	58.3	68.4
Subsystem motoring efficiency considering battery energy only, $n_{sb} = 100 \times E_{ta}/E_b$, percent	52.2	60.0	69.8
Distance traveled per cycle, km (mi)	0.362 (0.225)	0.595 (0.370)	1.65 (1.03)

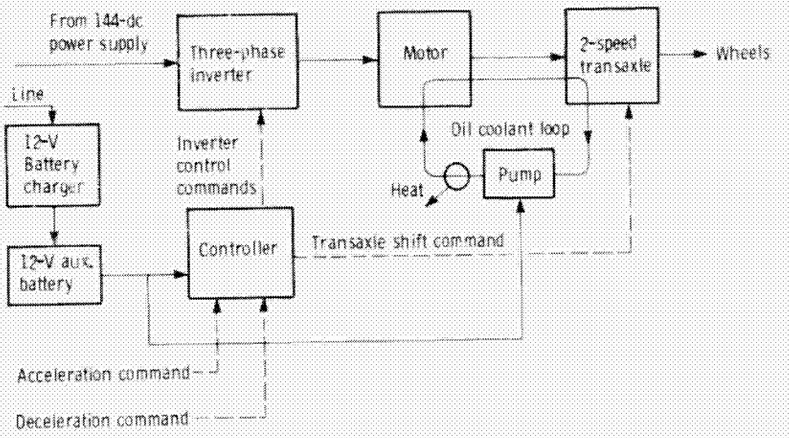

Figure 1. - Experimental ac propulsion subsystem block diagram.

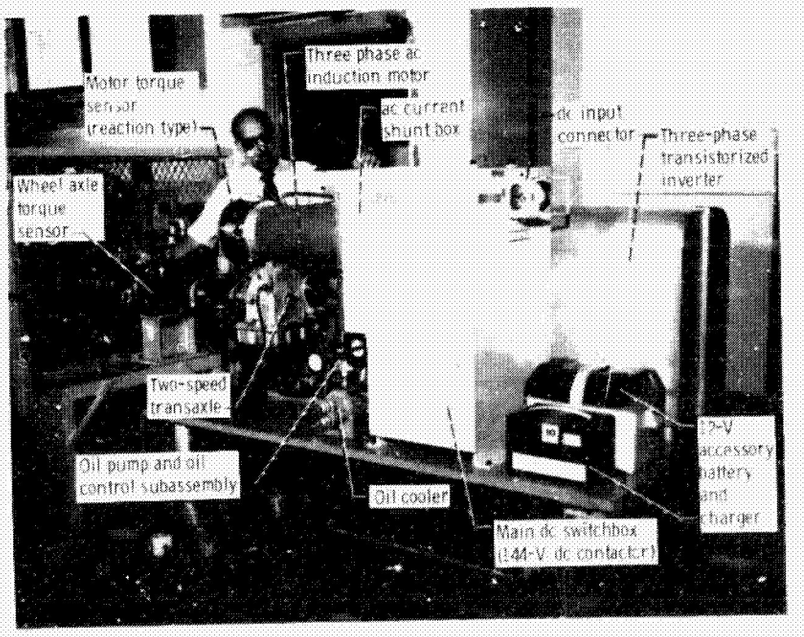

Figure 2. - Experimental propulsion subsystem breadboard installed on the Lewis road load simulator.

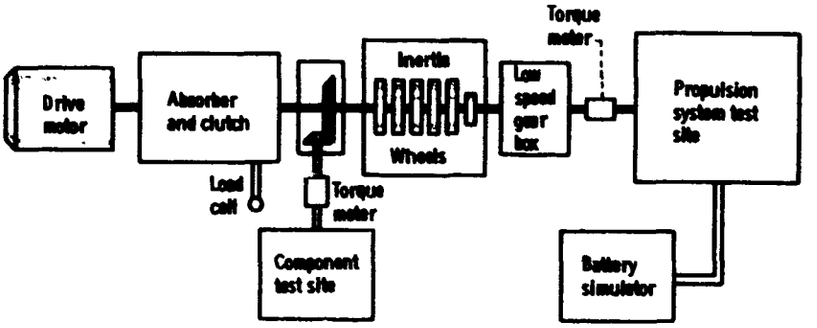

Figure 3. - Road load simulator schematic.

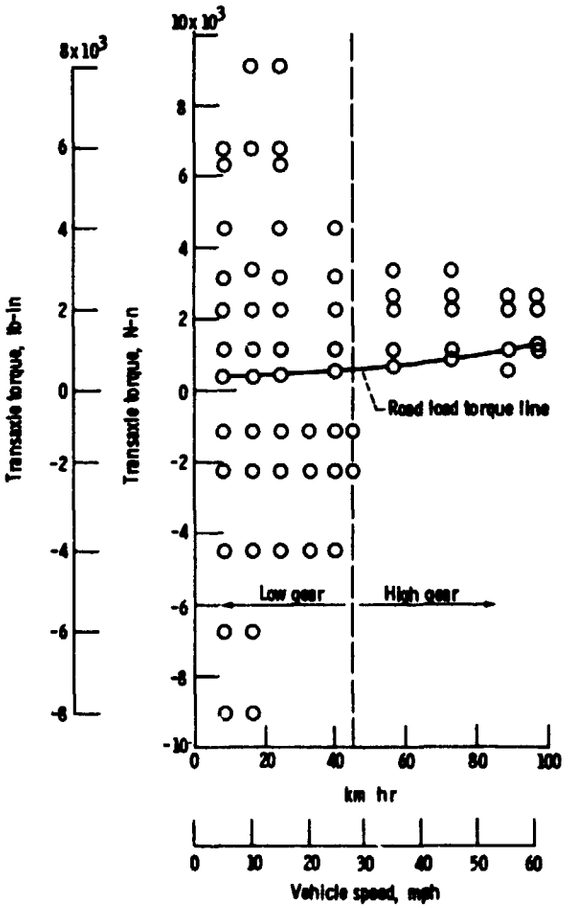

Figure 4. - Steady-state-speed torque test points.

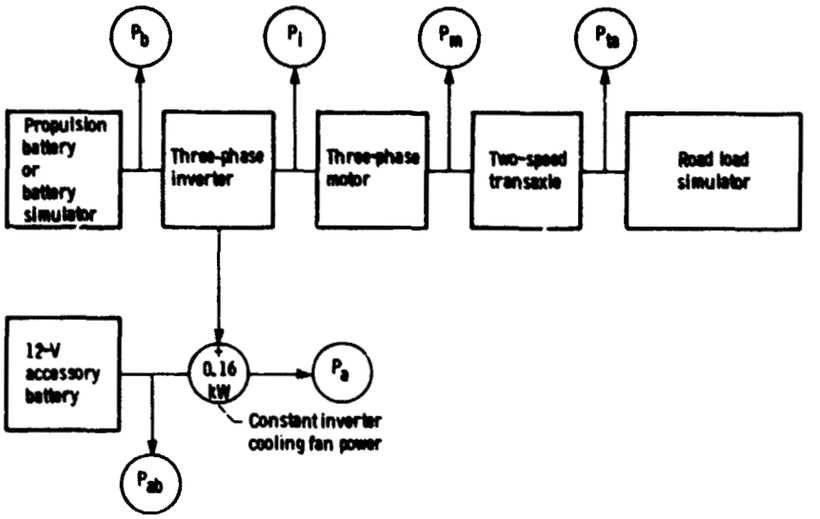

Figure 5. - Power flow measurement.

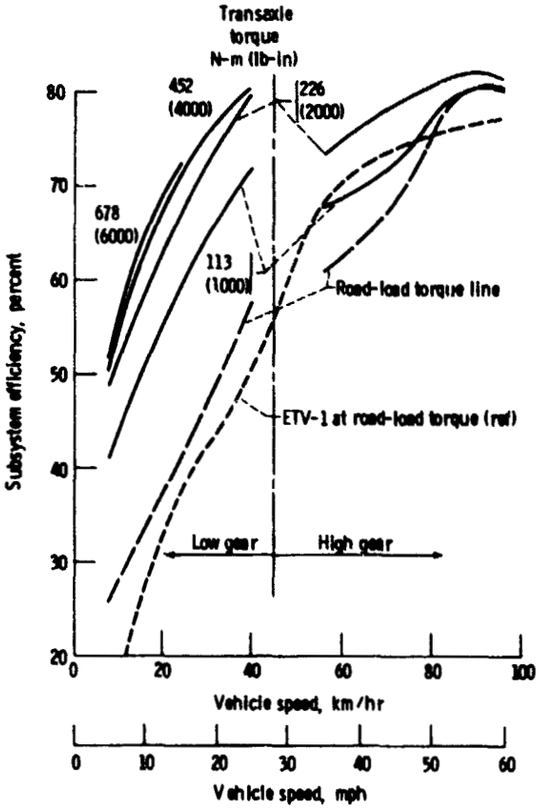

Figure 6. - Subsystem efficiency for constant transaxle torque. Battery simulator voltage, 144 V; motor temp, 43.3 °C (110 °F).

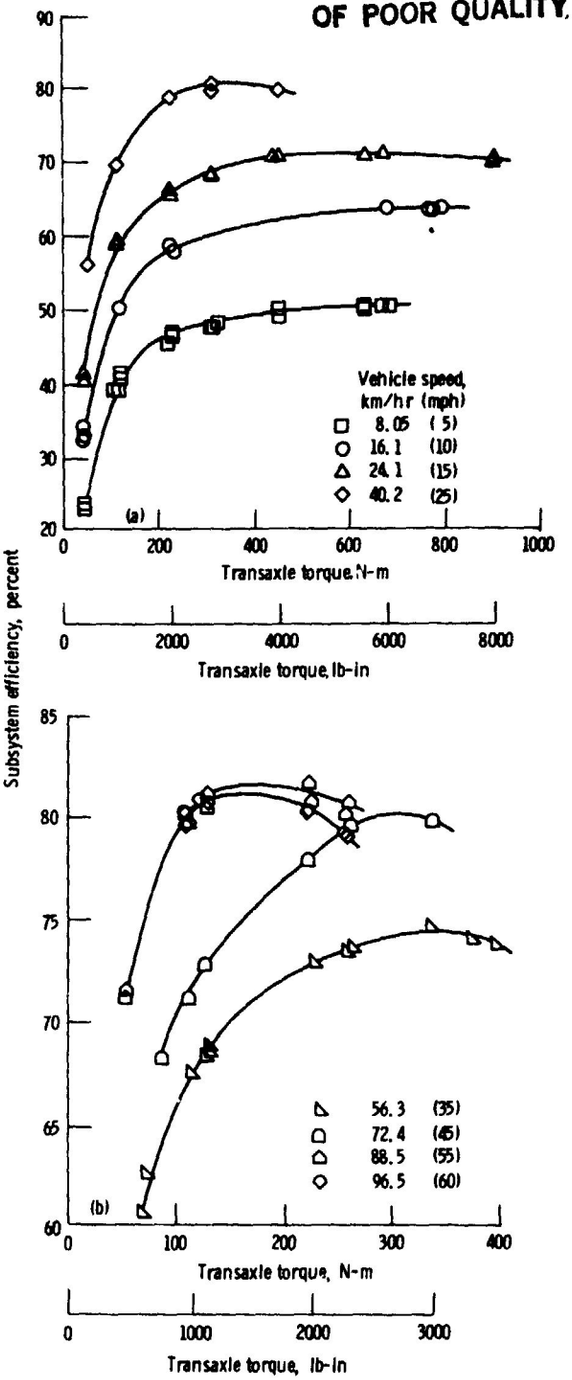

(a) Low-gear-speed range.

(b) High-gear-speed range.

Figure 7. - Subsystem efficiency as a function of transaxle torque for constant vehicle speeds. Battery simulator voltage, 144 V motor temperature, 65.6 ^{0}C (150 ^{0}F).

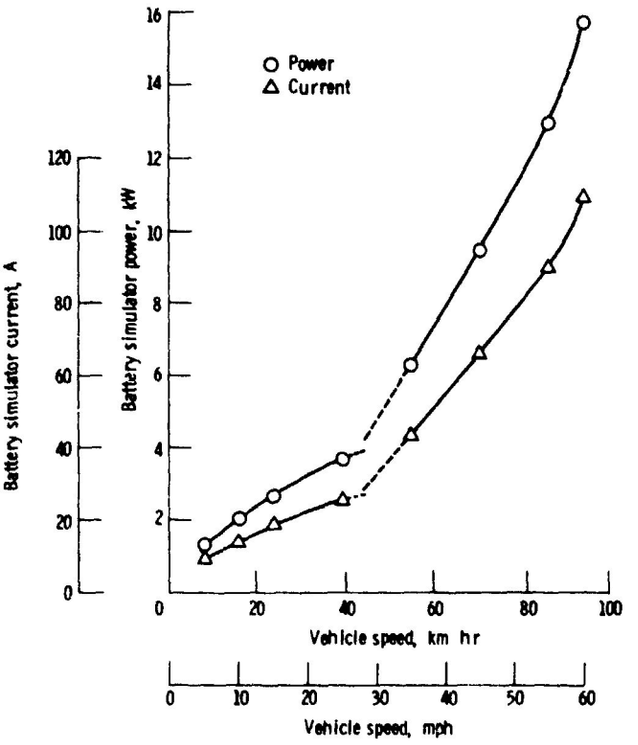

Figure 8. - Battery simulator power and current as functions of steady vehicle speed. Battery simulator voltage, 144 V; motor temperature, 65.5° C (150° F).

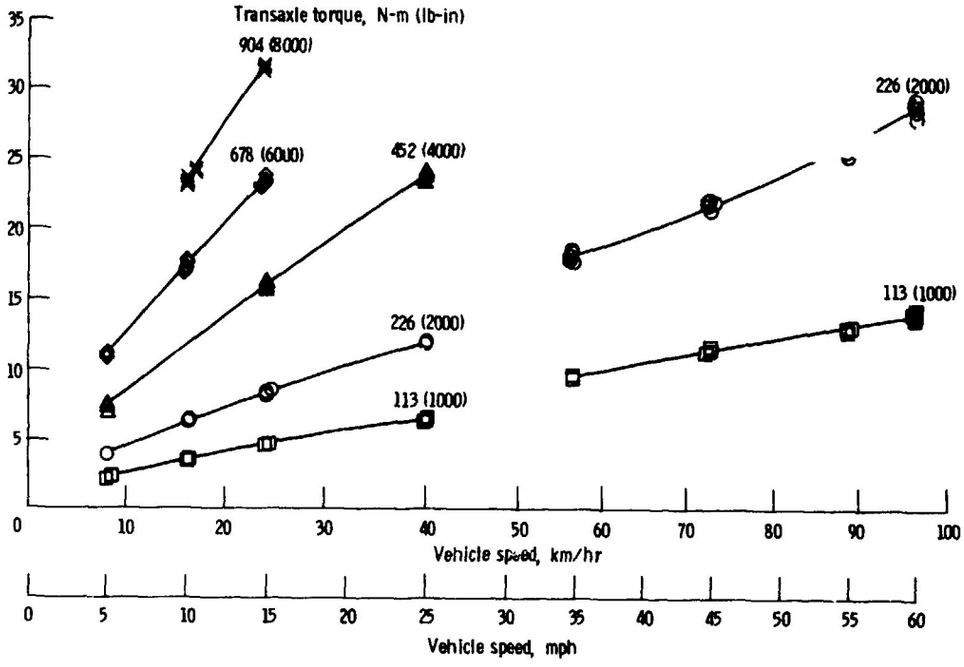

Figure 9. - Battery simulator power as a function of vehicle speed on lines of constant transaxle torque. Battery simulator voltage, 144 V.

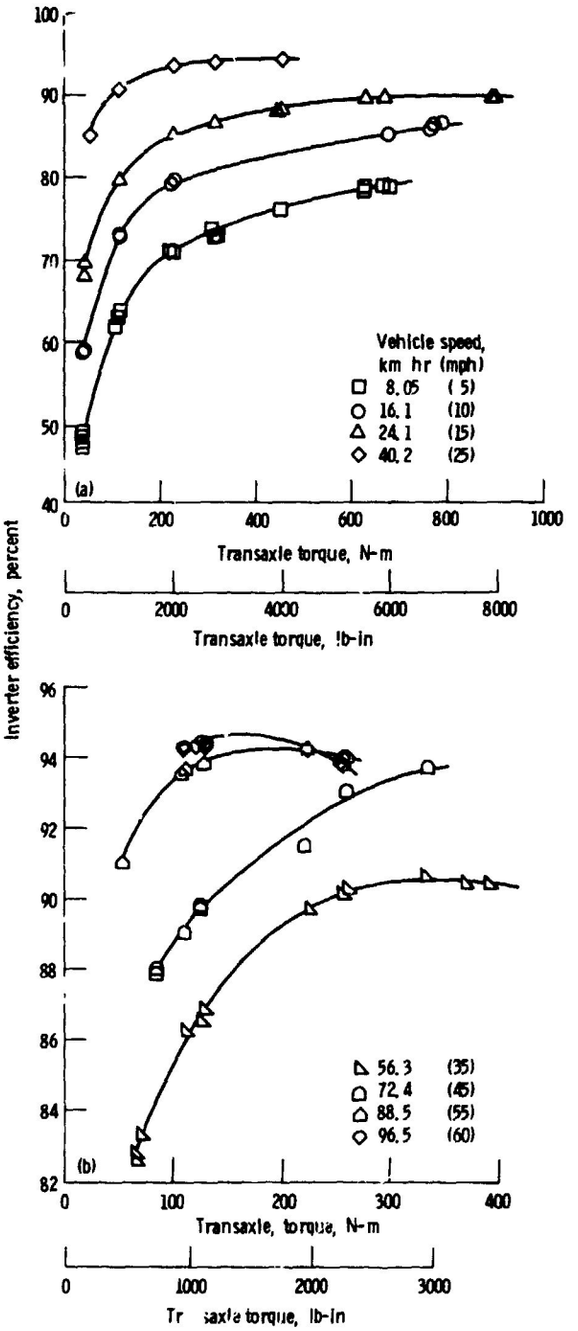

(a) Low-gear-speed range.

(b) High-gear-speed range.

Figure 10. - Inverter efficiency as function of transaxle torque on lines of constant vehicle speed. Battery simulator voltage, 144 Vdc; motor temperature, 65.6 °C (150 °F).

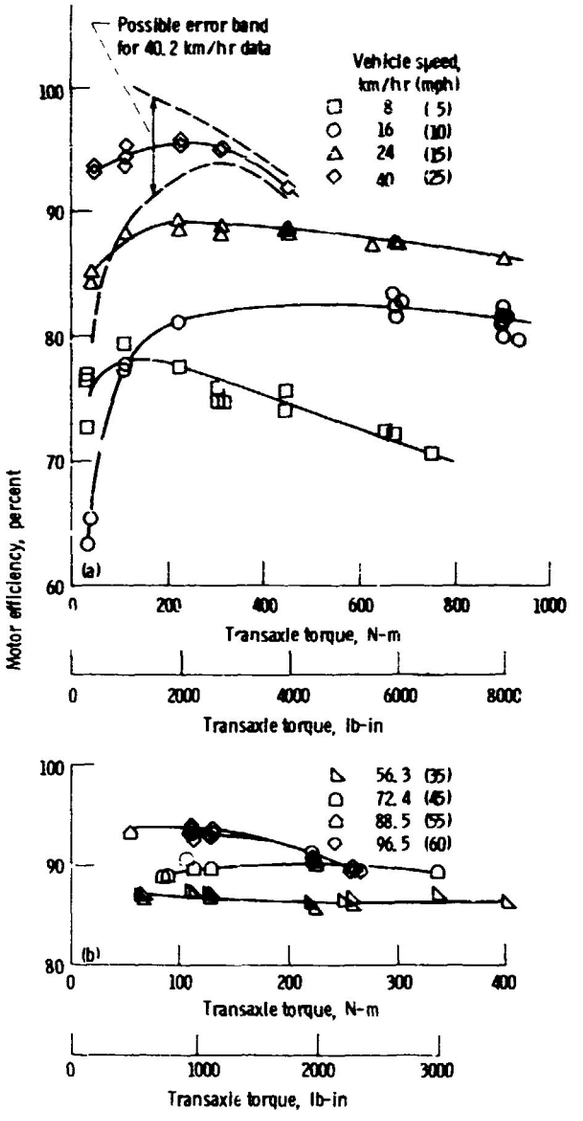

(a) Low-gear-speed range.

(b) High-gear-speed range.

Figure 11. - Motor efficiency as function of transaxle torque for constant vehicle speed. Battery simulator voltage, 144 V; motor temperature, 37.8 ^{0}C (100 ^{0}F).

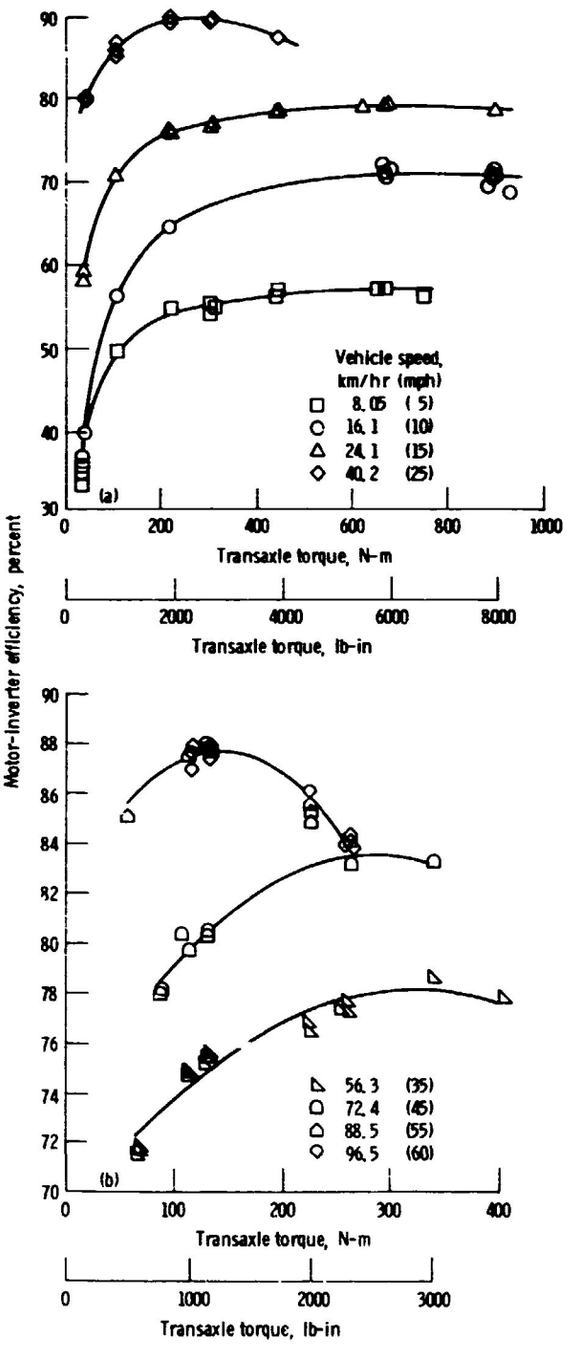

(a) Low-gear-speed range.

(b) High-gear-speed range.

Figure 12. - Combined motor-inverter efficiency as a function of transaxle torque on lines of constant vehicle speed. Battery simulator voltage, 144 Vdc; motor temperature, 37.8 °C (100 °F).

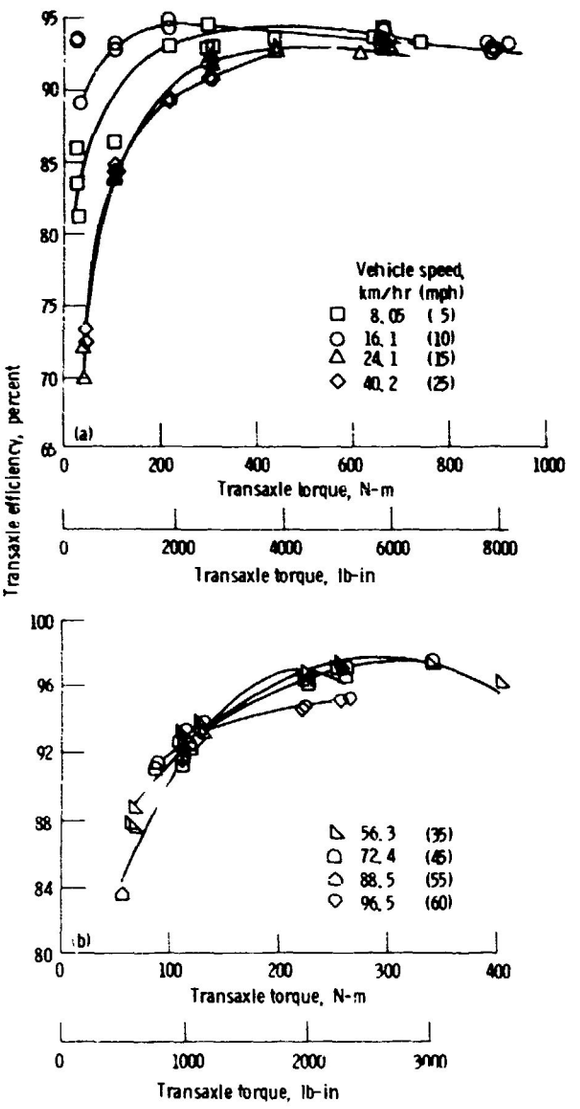

(a) Low-gear-speed range.

(b) High-gear-speed range.

Figure 13. - Transaxle efficiency as a function of transaxle torque on lines of constant vehicle speed. Battery simulator voltage, 144 Vdc: motor temperature, 37.8 ^{0}C (100 ^{0}F).

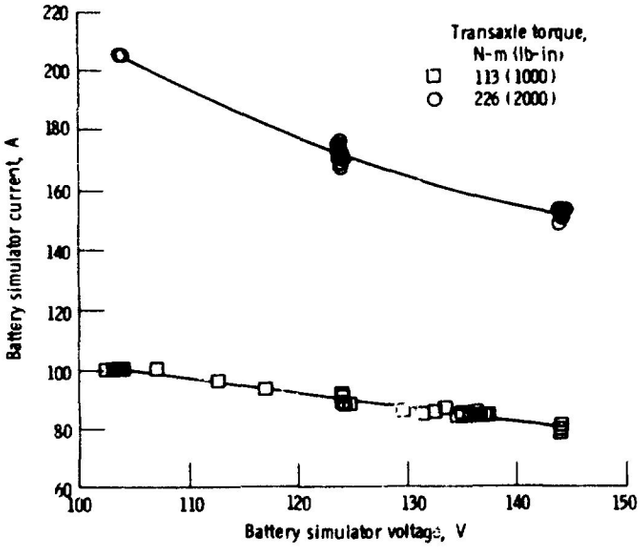

Figure 14. - Battery simulator current as a function of battery simulator voltage on lines of constant transaxle torque. Vehicle speed, 72.4 km/hr (45 mph).

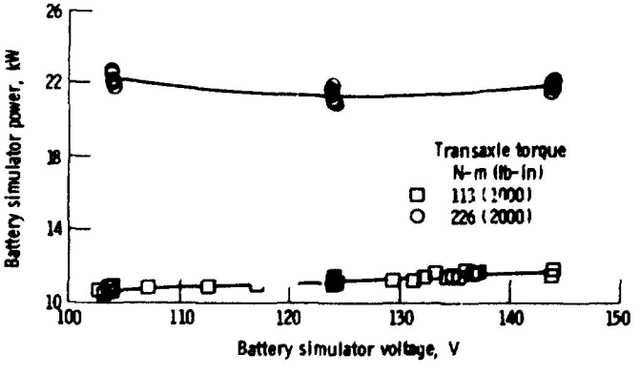

Figure 15. - Battery simulator power as a function of battery simulator voltage on lines of constant transaxle torque. Vehicle speed, 72.4 km/hr (45 mph).

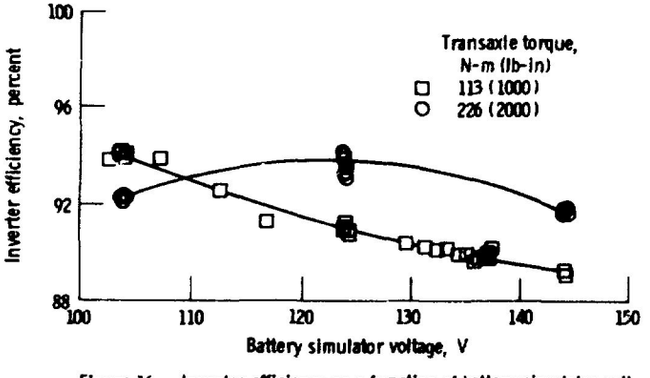

Figure 16. - Inverter efficiency as a function of battery simulator voltage on lines of constant transaxle torque. Vehicle speed, 72.4 km/hr (45 mph).

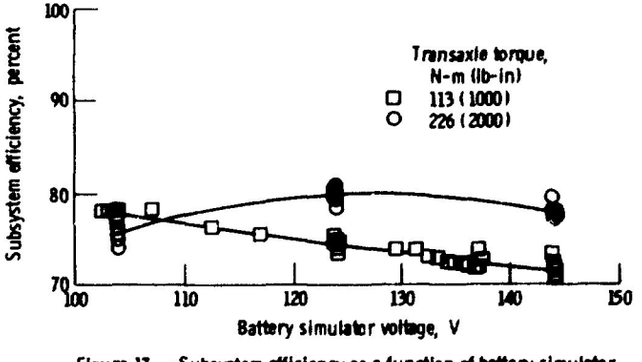

Figure 17. - Subsystem efficiency as a function of battery simulator voltage on lines of constant transaxle torque. Vehicle speed, 72.4 km/hr (45 mph).

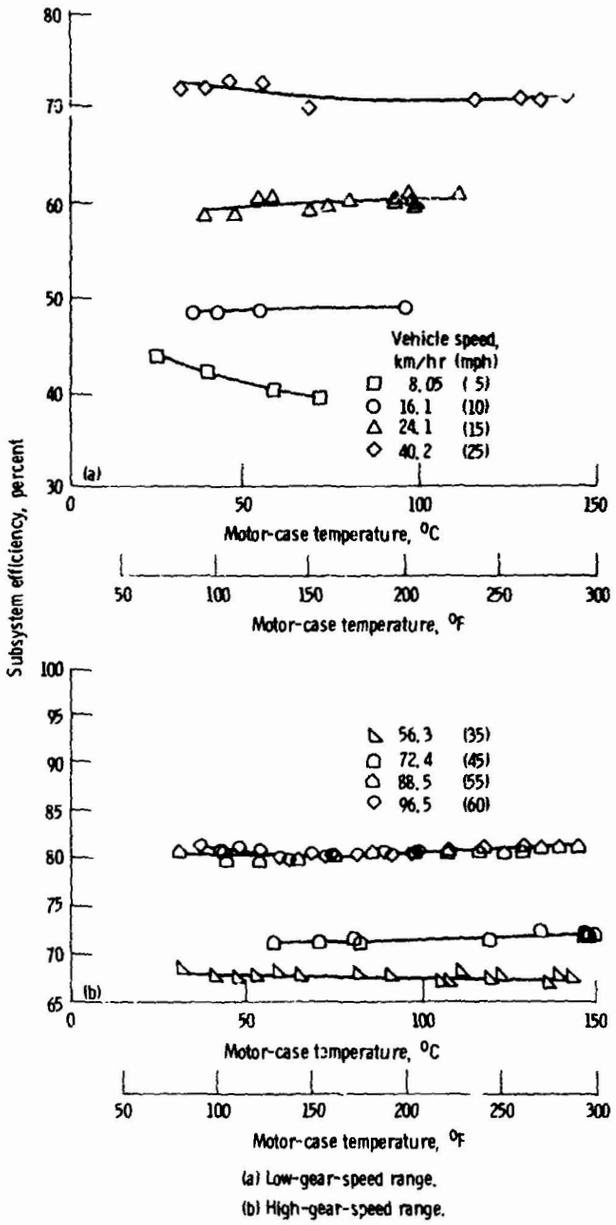

(a) Low-gear-speed range.

(b) High-gear-speed range.

Figure 18. - Subsystem efficiency as a function of motor case temperature on lines of constant vehicle speed. Battery simulator voltage, 144 V; transaxle torque, 113 N-m (1000 lb-in).

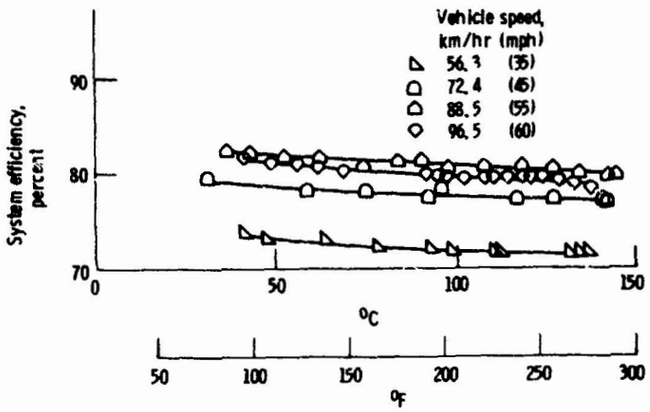

Figure 19. - System efficiency as a function of motor case temperature on lines of constant vehicle speed in high gear range. Battery voltage, 144 V; transaxle torque, 226 N-m (2000 lb-in).

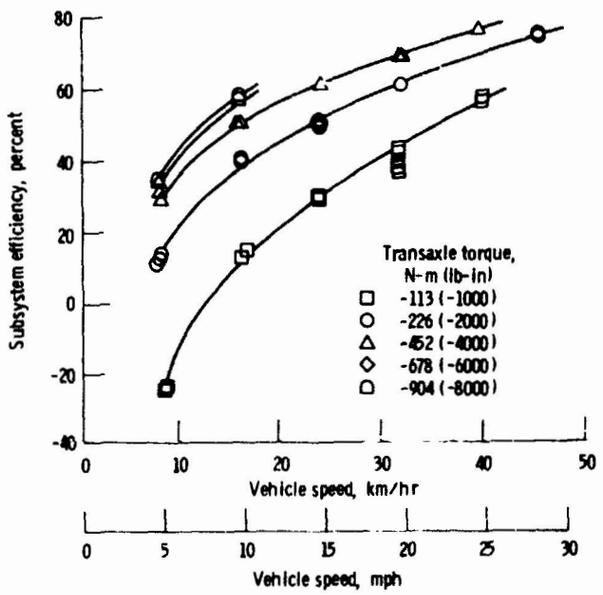

Figure 20. - Regenerative braking subsystem efficiency as a function of vehicle speed on lines of constant transaxle torque for the low-gear-speed range.

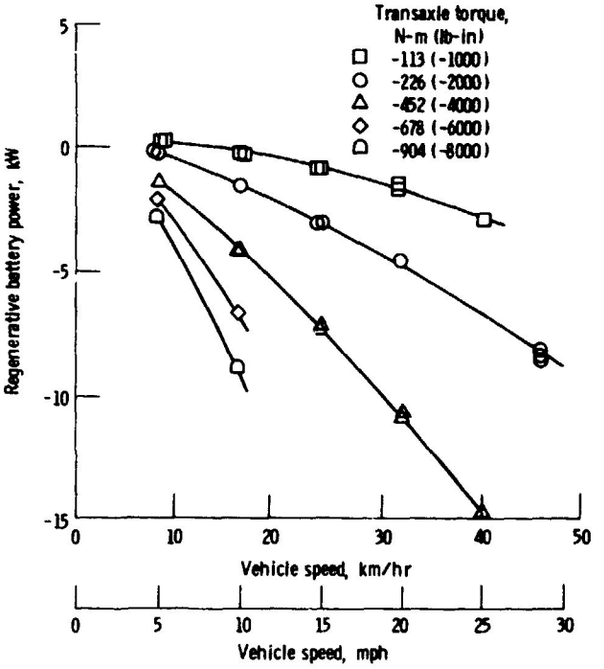

Figure 21. - Regenerative battery power as a function of vehicle speed on lines of constant transaxle braking torque for the low-gear-speed range.

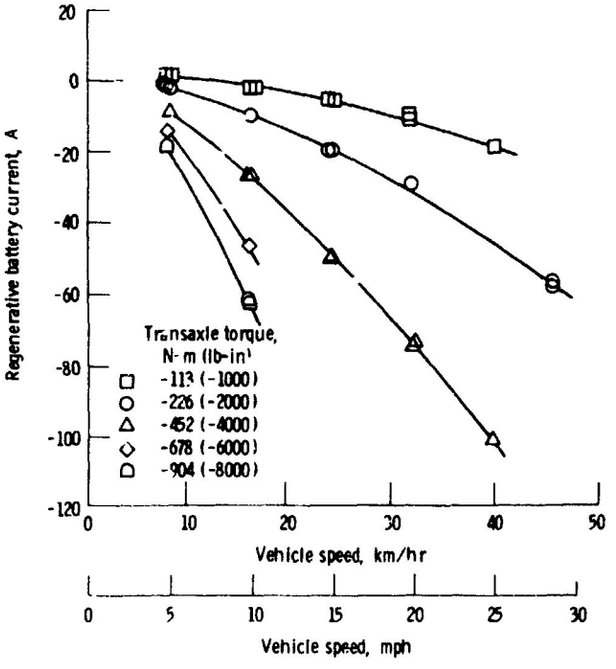

Figure 22. - Regenerative battery current as a function of vehicle speed on lines of constant transaxle braking torque for the low-gear-speed range.

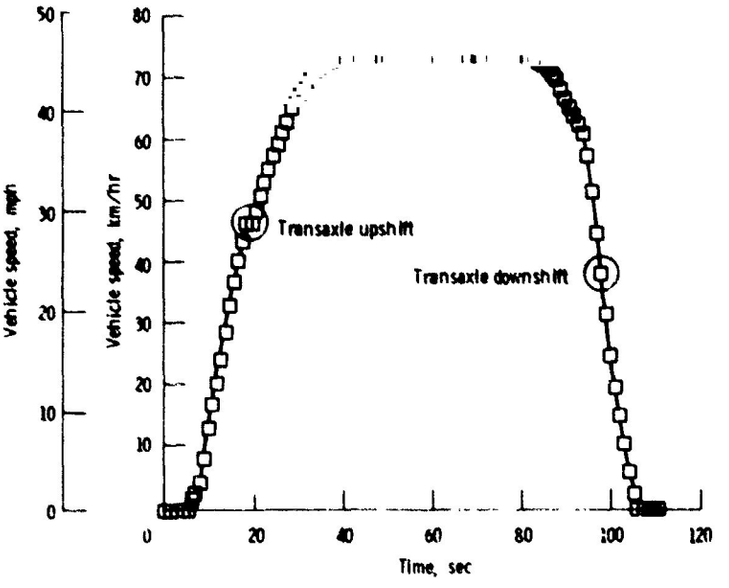

Figure 23. - Vehicle speed as a function of time over a schedule D cycle.

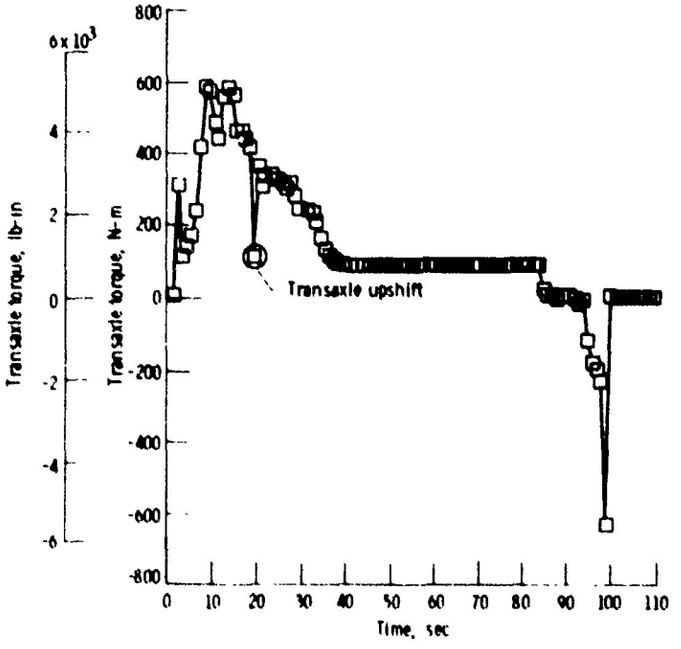

Figure 24. - Transaxle torque as a function of time over a schedule D cycle.

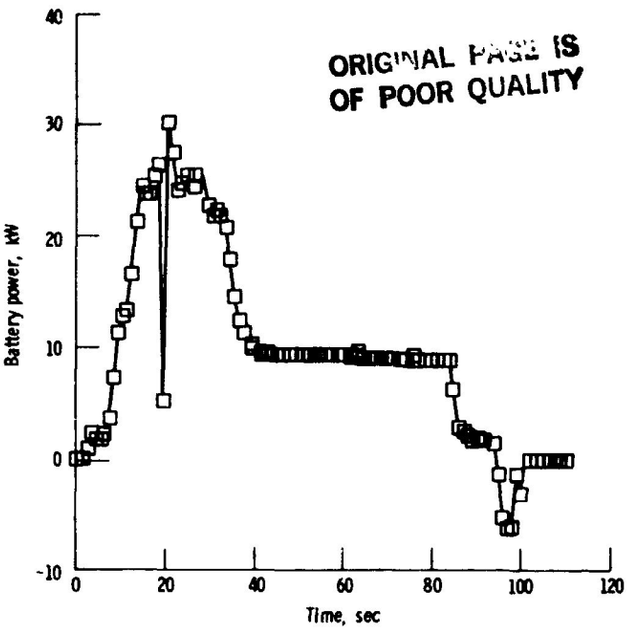

Figure 25. - Battery power as a function of time over a schedule D cycle.

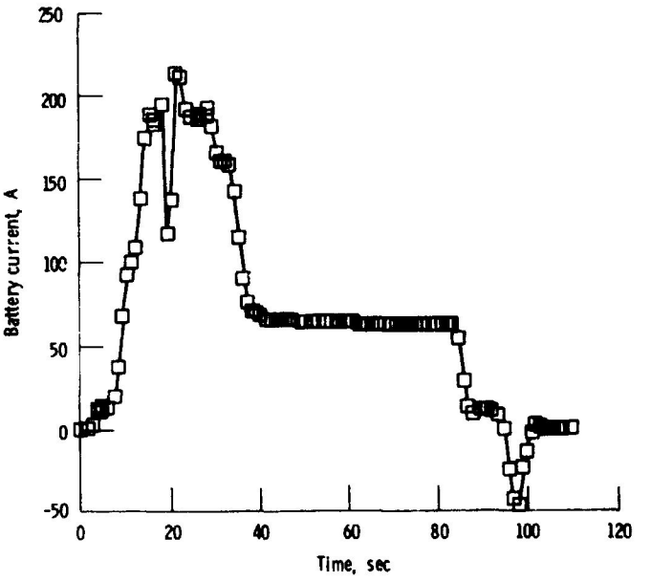

Figure 26. - Battery current as a function of time over a schedule D cycle.

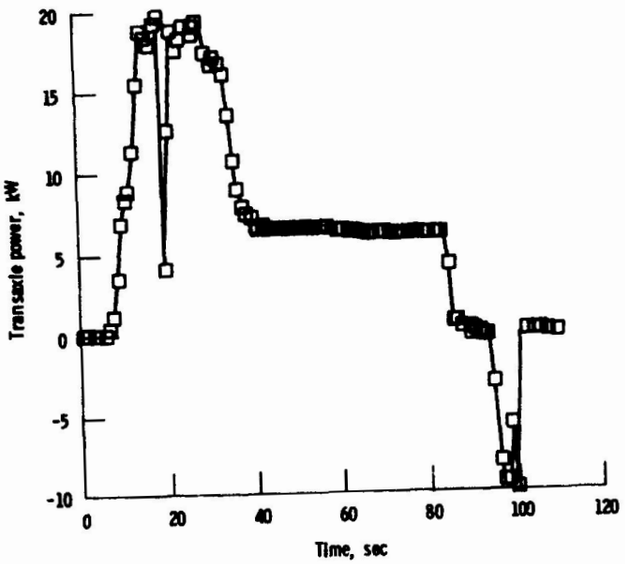

Figure 27. - Transaxle power as a function of time over a schedule D cycle.

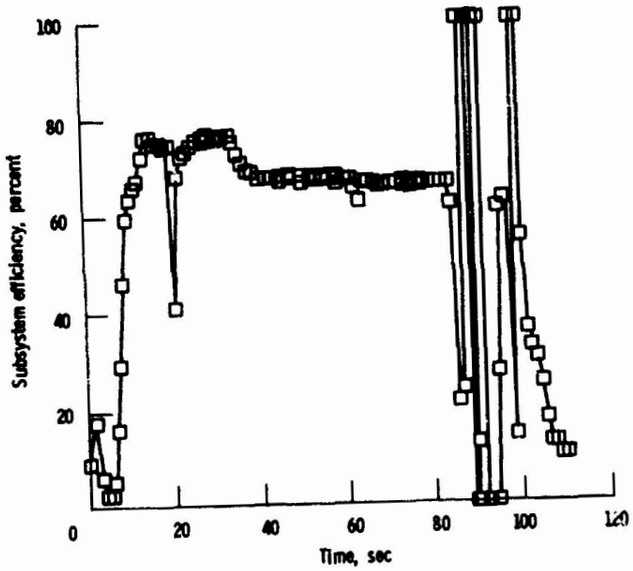

Figure 28. - Subsystem efficiency as a function of time over a schedule D cycle.

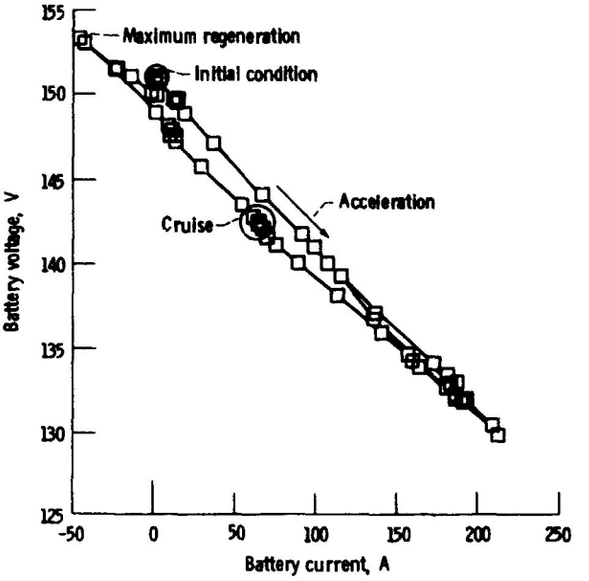

Figure 29. - Battery voltage-current characteristic over a schedule D cycle. Average battery temperature, 31.3 °C (88.4 °F); battery SOC, 92 percent full.

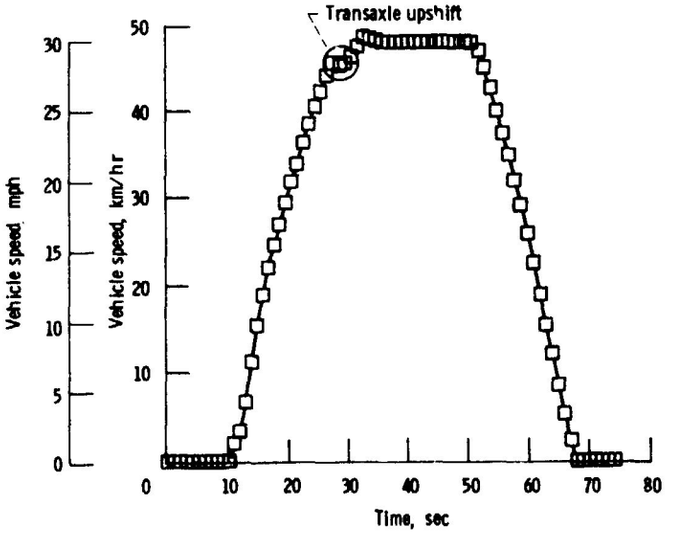

Figure 30. - Vehicle speed as a function of time over a schedule C cycle.

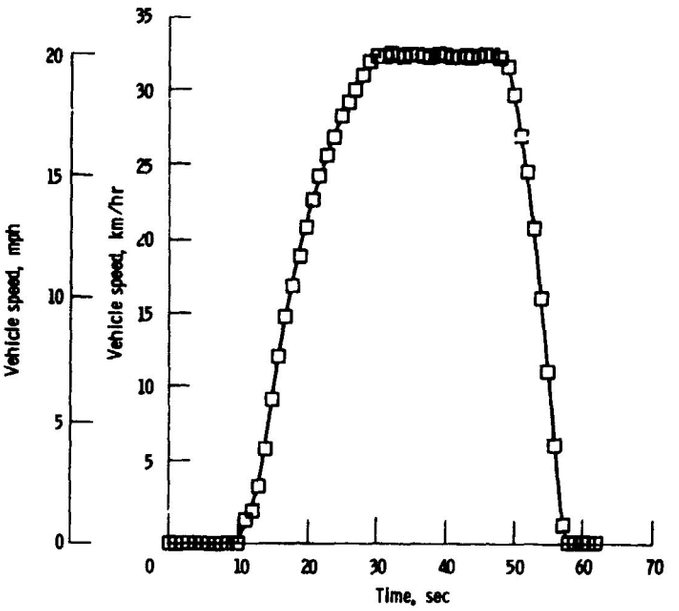

Figure 31. - Vehicle speed as a function of time over a schedule B cycle.

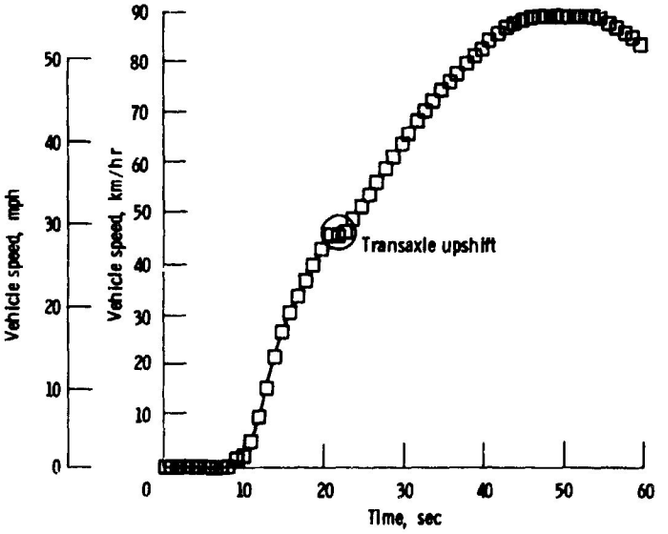

Figure 32. - Maximum acceleration. Simulated road grade, 0%; battery SOC, 95%.

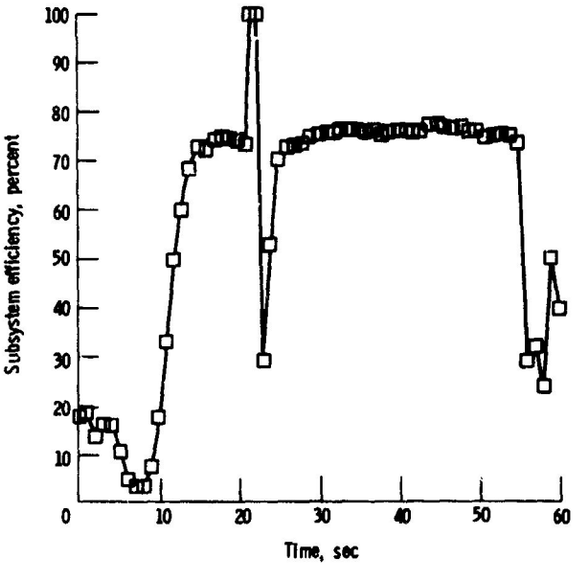

Figure 33. - Subsystem efficiency as a function of time during maximum acceleration to 88.5 km/hr (55 mph). Simulated road grade, 0%; battery SOC, 95%.

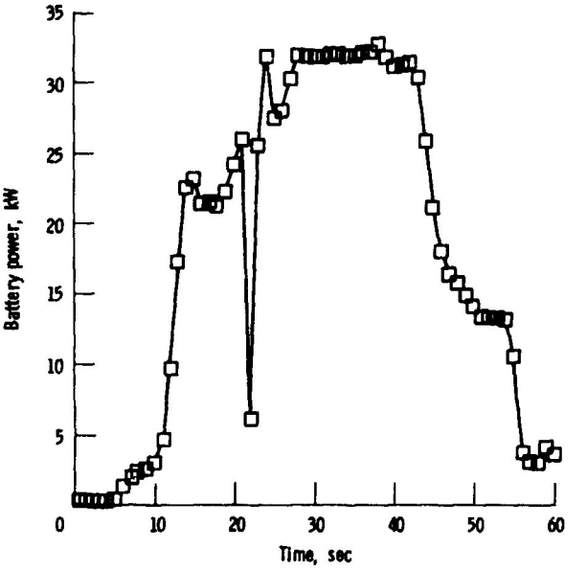

Figure 34. - Battery power as a function of time during maximum acceleration to 88.5 km/hr (55 mph). Simulated road grade, 0%; battery SOC, 95%.

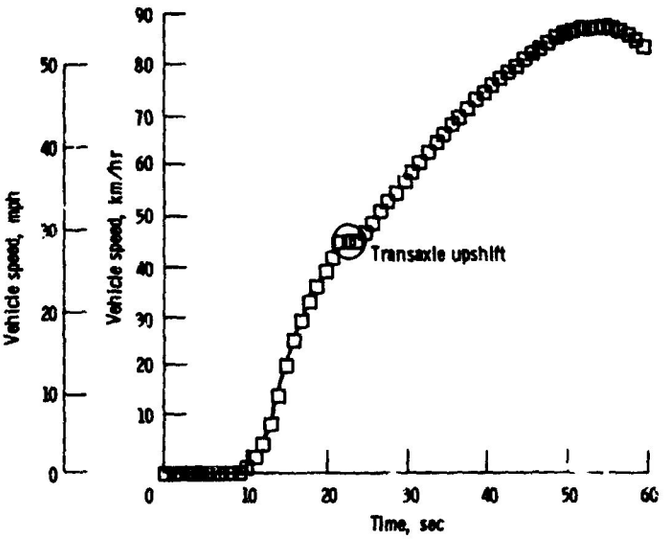

Figure 35. - Vehicle speed as a function of time during a maximum acceleration on a 4-percent grade. Battery 20C, 100%.